HHS Public Access

Author manuscript

*Mol Cancer Res*. Author manuscript; available in PMC 2020 February 01.

Published in final edited form as:

*Mol Cancer Res*. 2019 February ; 17(2): 370–383. doi:10.1158/1541-7786.MCR-18-0670.

# UNC-45A is a Novel Microtubule-associated Protein and Regulator of Paclitaxel Sensitivity in Ovarian Cancer Cells

**Ashley Mooneyham**[1], **Yoshie Iizuka**[1], **Qing Yang**[2], **Courtney Coombes**[2], **Mark McClellan**[2], **Vijayalakshmi Shridhar**[3], **Edith Emmings**[1], **Mihir Shetty**[1], **Liqiang Chen**[4], **Teng Ai**[4], **Joyce Meints**[5], **Michael K Lee**[5], **Melissa Gardner**[2], and **Martina Bazzaro**[1,*]

[1]Masonic Cancer Center and Department of Obstetrics, Gynecology and Women's Heath, University of Minnesota, Minneapolis, MN 55455, USA,

[2]Department of Genetics, Cell Biology, and Development, University of Minnesota, Minneapolis, MN 55455,

[3]Department of Experimental Pathology, Mayo Clinic College of Medicine, Rochester, MN 55905 USA,

[4]Center for Drug Design, Academic Health Center, University of Minnesota, Minneapolis, MN 55455 USA,

[5]Department of Neuroscience, University of Minnesota Minneapolis, MN 55455 USA.

## Abstract

UNC-45A, a highly conserved member of the UCS (UNC45A/CRO1/SHE4P) protein family of co-chaperones, plays an important role in regulating cytoskeletal-associated functions in invertebrates and mammalian cells including cytokinesis, exocytosis, cell motility, and neuronal development. Here, for the first time UNC-45A is demonstrated to function as a mitotic-spindle-associated protein that destabilizes microtubules (MTs) activity. Using *in vitro* biophysical reconstitution and total internal reflection fluorescence (TIRF) microscopy analysis, reveal that UNC-45A directly binds to taxol-stabilized MTs in the absence of any additional cellular co-factors or other microtubule-associated proteins (MAPs) and acts as an ATP-independent microtubule destabilizer. In cells, UNC-45A binds to and destabilizes mitotic spindles and its depletion causes severe defects in chromosome congression and segregation. UNC-45A is overexpressed in human clinical specimens from chemoresistant ovarian cancer and that UNC-45A overexpressing cells resist chromosome mis-segregation and aneuploidy when treated with clinically relevant concentrations of paclitaxel. Lastly, UNC-45A depletion exacerbates paclitaxel-mediated stabilizing effects on mitotic spindles and restores sensitivity to paclitaxel.

*Corresponding author: Martina Bazzaro, Masonic Cancer Center, 420 Delaware Street S.E, Room 490, Minneapolis, Minnesota 55455, Tel: 612-6252889, Fax: 612-626-0665, mbazzaro@umn.edu.

Author contributions

Ashley Mooneyham, Qing Yang, Yoshie Iizuka, Courtney Coombes, Mihir Shetty, Edith Emmings, Mark Mc Clellan, Liqiang Chen, Teng Ai, and Joyce Meints performed the experiments and analyzed the data. Ashley Mooneyham, Viji Shridhar, Michael K Lee, Melissa Gardner and Martina Bazzaro, designed the experiments, analyzed the data and wrote the manuscript.

Disclosure of Potential Conflict of Interest

No potential conflicts of interest were disclosed.

**Keywords**

UNC-45A; paclitaxel; human cancers; chemoresistance

## Introduction

The uncoordinated protein 45 (UNC-45) is a member of the UCS protein family (UNC-45/CRO1/She4p) of myosin co-chaperones highly conserved throughout evolution [1–7]. While UNC-45 conservation suggests it has critical importance, its functions are still largely unknown. We and others have contributed to the understanding of the role of UNC-45A in mammalian cells within and outside its regulation of myosin activity. UNC-45A has been shown to control myoblast cell proliferation and its levels to drop as differentiation occurs [2]. Recently UNC-45A has been shown to promote myosin folding and stress fiber assembly [8]. We have shown that UNC-45A controls non-muscle myosin II (NMII)-associated functions in ovarian cancer cells [9], immune cells [10] and neurons [11] via regulating NMII activation and its binding to actin. We and others have also shown that in breast and ovarian cancers, UNC-45A is a cell cycle associated protein whose expression pattern correlates with poor clinical outcome [9, 12].

In cervical cancer cells, UNC-45A has been shown to regulate the progesterone receptor/Hsp90 pathway [13]. Furthermore, co-localization and cellular fractionation studies using cervical cancer cells have revealed that UNC-45A is a novel centrosomal-associated protein [14]. This, along with the fact that UNC-45A overexpression correlates with poor outcome in human cancers [9, 12], and that a significant contributor to poor patient outcomes is chemoresistance to the microtubule-stabilizing chemotherapy agent paclitaxel [15, 16], suggests that UNC-45A may play a role in regulating microtubule stability.

In this study we show for the first time that UNC-45A overexpression is associated with paclitaxel resistance but not carboplatin resistance in ovarian cancer cell lines and clinical specimens of human ovarian tumors. We also show that UNC-45A is a mitotic-spindle-associated protein, and that UNC-45A overexpressing cancer cells escape chromosomal missegregation and aneuploidy when exposed to paclitaxel. Furthermore, UNC-45A depletion results with mitotic defects characterized by improper chromosome congression, segregation, and presence of multipolar spindles caused by hyperstable microtubules. Mechanistically, Total Internal Reflection Fluorescence (TIRF) microscopy analysis revealed that UNC-45A is a microtubule destabilizing protein capable of depolymerizing otherwise stable, paclitaxel-treated microtubules in absence of any other cellular components. Lastly, we show that UNC-45A restores the sensitivity of cancer cells to clinically relevant concentrations of paclitaxel via exacerbating paclitaxel-mediated stabilizing effects on cancer cells' mitotic spindles. Taken together our studies support the role of UNC-45A as a novel member of the MT destabilizing protein family and as a molecular target for paclitaxel-resistant human cancers.

## Materials and Methods

### Chemicals

The 2,3-bis[2-methoxy-4-nitro-5-sulfophenyl]-2H-tetrazolium-5-carboxanilide inner salt (WST-1) was purchased from Cayman Chemicals. Propidium iodide (PI) was purchased from Sigma. 4',6-diamidino-2-phenylindole (DAPI) was purchased from Invitrogen. Paclitaxel was purchased from Teva Pharmaceuticals and Carboplatin was purchased from Segent Pharmaceuticals. Ro 3306 was purchased from Abcam.

### Cell lines

The ovarian cancer cell line COV362 was a generous gift from Dr. Panagiotis A. Konstantinopoulos (Dana Farber Cancer Institute). The ovarian cancer cell lines OVSAHO, Kuramochi, and JHOS2 were a generous gift from Dr. Douglas Levine (Memorial Sloan Kettering Cancer Center). The ovarian cancer cell line SKOV-3, the cervical cancer cell line HeLa and the fibroblast cell line NIH3T3 were purchased from the American Type Culture Collection (ATCC). Cell lines were cultured in DMEM supplemented with 10% fetal bovine serum.

### Antibodies

Anti UNC-45A (Enzo Life Sciences), anti alpha-tubulin (Sigma), anti acetylated-alpha-tubulin (Santa Cruz Biotechnology), anti ɣ-tubulin (Sigma) anti MCAK (GeneTex). Peroxidase-linked anti-mouse Immunoglobulin G and peroxidase-linked anti-rabbit Immunoglobulin G were from Amersham. Texas Red-Goat anti-Mouse IgG, Texas Red-Goat anti-Rabbit IgG, FITC-Donkey and anti-Mouse IgG, Peroxidase-Goat anti-mouse IgG, Peroxidase–Goat anti-rabbit IgG were purchased from Jackson Immunoresearch Laboratories, Inc.

**Modulation of UNC-45A expression levels in cells.—**For UNC-45A silencing or overexpression, scramble and UNC-45A shRNAs lentiviral supernatant or empty vector control and UNC-45A-GFP lentiviral supernatants were prepared and used to infect HeLa, Fibroblasts, COV362 and SKOV-3 cell lines as we have previously described[10, 11]. MCAK silencing was obtained via transfection with siRNA-MCAK (Ambion).

### Immunofluorence microscopy, image acquisition, and quantification

Cells were fixed in methanol for 5 minutes at −20°C. After blocking with 5% BSA in PBST, cells were stained with anti-UNC-45A, anti-α tubulin, anti-ɣ tubulin or anti- acetylated α-tubulin primary antibodies followed by FITC- or Texas Red-conjugated secondary antibodies and analyzed via confocal fluorescence microscopy. Images were taken with an Olympus BX2 upright microscope equipped with a Fluoview 1000 confocal scan head. A UPlanApo N 60X/1.42 NA objective was used. FITC was excited with a 488 nm laser and emission collected between 505 and 525 nm. For Texas Red a 543 nm laser was used for excitation and emission collected between 560 and 660 nm. Images were taken with sequential excitation. For all mitotic phenotype comparisons, analyzed cells were taken from same experiment dates with identical acquisition settings. Cells were synchronized using 5μM of Ro3306 for 20 hours followed by rescue with DMEM + 10% FBS. Images were

analyzed using ImageJ software. Pole to pole distance was measured from the center of one pole, as identified by gamma tubulin staining, to the center of the next pole. Chromosome congression was measured from the widest metaphase plate area of each cell. Misaligned chromosomes were defined as chromosomes with a clear separation from the metaphase plate. Lagging chromosomes were defined as chromosomes trailing behind newly separated DNA in anaphase cells. Fluorescent intensity of the mitotic spindle was measured within a defined circular area containing the entirety of each spindle pole using ImageJ software.

**Western blot analysis and immunoprecipitation.—**Total cellular protein (10–40 μg) from each sample was separated by SDS-PAGE, transferred to PVDF membranes and subjected to Western blot analysis. For co-immunoprecipitation, cells were lysed in lysis buffer (50 mM Tris, pH 7.4, 150 mM NaCl, 1% Nonidet P-40, 1 × protease inhibitor mixture, 1 x phosphatase inhibitor mixture), pre-cleared and precipitated with primary antibody and Protein A/G beads. Samples were subjected to Western blot analysis using the specified antibodies. Per each protein, Western blots were quantified within the linear range of detection (Supplementary Figure 8).

**Microtubule cosedimentation assay in cells.—**Cells were lysed using 1% NP-40 lysis buffer containing 150 mM NaCl, 50 mM Tris-HCl pH 7.8, and protease inhibitor cocktail. The lysates were treated with either control DMSO or 1μM of taxol and incubated at 37°C for an hour. Lysates were spun at 15,000rpm for 30 minutes at room temperature and the supernatant and pellet fractions were separated by SDS-PAGE and analyzed via Western blotting. Extent of UNC-45A association with polymerized microtubules (pellet fraction) was determined by densitometric analysis using imageJ software.

**Recombinant protein.—**GFP-UNC-45A was cloned into pGEX-2TK to generate the GST-GFP-UNC-45A protein. The protein was expressed in Rosetta (DE3) pLysS and following GST removal it was affinity purified and dialyzed as we have previously described [17, 18].

## Preparation of paclitaxel-stabilized microtubules

The paclitaxel-stabilized microtubules were prepared in a mixture that consisted of 8.3 μM rhodamine-labeled tubulin, 24.7 μM unlabeled tubulin, 1 mM GTP, 4 mM $MgCl_2$, and 4% DMSO. The mixture was kept on ice for 5 minutes followed by a 30-minute incubation at 37°C. After incubation, the mixture containing microtubules was diluted into 390 μL warm Brb80 solution containing 10 μM Paclitaxel. The microtubules were then spun down at 20 psi for 5 minutes. The microtubule pellet was then resuspended into 400 μL warm 10 μM-Paclitaxel Brb80 solution and stored in 37°C incubator. All microtubules were prepared on the day of experiment.

## UNC-45A-GFP microtubule binding and depolymerization assay

The paclitaxel-stabilized microtubules were prepared and flowed into the imaging chamber as we have previously described [17, 18]. A final reaction mixture, containing 1x imaging buffer and 0.6 or 1.2 μM final concentration of UNC-45A-GFP, was then introduced into the imaging chamber and the interaction between UNC-45A-GFP and Paclitaxel-stabilized

microtubule was visualized via 488 nm and 561 nm lasers generated from Nikon™ TI-TIRF-PAU illuminator, which provided Total Internal Reflection Fluorescence (TIRF) illumination. The images were collected from a Nikon™ CFI Apo TIRF 100x oil objective using an Andor™ iXon EMCCD camera. The timelapse image collection was carried out automatically with 2.5-minute intervals for 1 hour at 10 preset locations on the imaging chamber. Laser power and exposure time were minimized while TIRF angle was maximized to avoid photobleaching and photodamage.

### UNC-45A-GFP microtubule depolymerization image analysis

Individual paclitaxel-stabilized microtubule images were cropped from the 1-hour timelapse image using ImageJ v1.49. The kymographs of individual microtubules were then generated using ImageJ to illustrate the depolymerization process over time. The change in microtubule length was then calculated and divided by the total time span of the process to obtain the depolymerization rate. The units were converted from horizontal and vertical pixels on the kymograph into μm and minutes, respectively. The data points gathered at the three experimental conditions (Control, 0.6 μM UNC-45A and 1.2 μM UNC-45A) were plotted separately in boxplots for comparison. Two-tailed Student's t tests were performed to illustrate the significance.

**Cell viability and proliferation rate assays.—**Cell viability was determined by 2,3-bis[2-methoxy-4-nitro-5-sulfophenyl]-2H-tetrazolium-5-carboxanilide inner salt assay as previously described[19]. Briefly, cells were seeded at the concentration of 1,000 per well in 100 μL medium in 96-well plate and treated with the indicated concentrations of drugs. At the indicated time points, cells were incubated according to the manufacturer's protocol with the WST-1 labeling mixture for 2 hours. Formazan dye was quantified using a spectrophotometric plate reader to measure the absorbance at 450nm (ELISA reader 190; Molecular Devices). Alternatively, cells were seeded in 6 well plates at a density of 30,000 cells per well and either mock treated or treated with 5nM of paclitaxel 24 hours post-plating. Proliferation rate was determined by counting the cells over a period of 6 days via Trypan blue exclusion staining.

**Measurements of intracellular levels of paclitaxel via High-Performance-Liquid-Chromatography (HPLC).—**COV362 ovarian cancer cells were grown in 10 cm dishes and treated with 100 nM of paclitaxel for 18 hours following which cells were trypsinized, pelleted, resuspended in 1 mL of ddH2O and stored at −80° C. Thawed cells were homogenized in water and the samples were applied to solid-phase extraction columns (Bond Elut C18, Agilent) and eluted with acetonitrile (1 mL). After the solvent was removed, the residue was lyophilized and reconstituted in the HPLC mobile phase (30% of 35 mM acetic acid in ddH2O and 70% acetonitrile, 100 μL). A 50 μL injection was separated using isocratic 30% of 35 mM acetic acid in ddH2O and 70% acetonitrile (2 mL/min) on an Agilent 1200 Infinity series HPLC system with a Gemini 5μ C18 110A 4.6 Å~ 250 mm column. The paclitaxel signal (retention time 4.6 min) was monitored at 227 nm. Analyses were performed independently in triplicate. A standard curve was generated using

untreated cell lysates that were spiked with paclitaxel in acetonitrile (250 nM to 100 μM, final concentrations) before solid-phase separation.

## Human Subjects

Archival tissues were used with the Institutional Review Board approval.

## Immunohistochemistry

Five-micron thick formalin-fixed, paraffin-embedded sections were deparaffinized and rehydrated by sequential washing with xylene, 100% ethanol, 95% ethanol, 80% ethanol, and PBS. For antigen retrieval, slides were immersed in Reveal Decloaker (Biocare Medical, Concord, CA) and steamed for 30 min at 100 degrees C. Endogenous peroxidase activity was blocked with 3% $H_2O_2$ for 10 min. After washing with PBS, slides were blocked with 10% normal goat serum in PBS for 10 min at room temperature, followed by incubation with rabbit anti-human polyclonal UNC-45 antibody (Proteintech Group Inc) at a concentration of 1:200 in blocking solution overnight at 4 degrees C. After washing twice with PBS, slides were incubated with a biotinylated anti-rabbit secondary antibody conjugated (10 min) and streptavidin/horseradish peroxidase (10 min; Dako), followed by 3,3-diaminobenzidine (Phoenix Biotechnologies) substrate for 3 min. Slides were lightly counterstained with Gill No. 3 hematoxylin (Sigma) for 60 s, dehydrated, and coverslipped. UNC-45A antibody validation was performed on COV-362 cell lines transduced with shRNA scramble or shRNA-UNC-45A and subject to immunohistochemistry as above described. Immunostained slides were reviewed by a panel of five investigators blinded to the clinical outcome of the corresponding patients. The staining intensity was rated as follows: 0 = no staining, 1+ = weak intensity, 2+ = moderate intensity, and 3+ = high intensity.

## Flow cytometry

Cell cycle status following treatment with drug or vehicle alone was determined via flow cytometry analysis in cells harvested at indicated time points, fixed and stained with 0.1% (m/v) propidium iodide in PBS-T. Fluorescence was measured with a FACSCantoII flow cytometer (Becton Dickinson) and analyzed with FlowJo software.

## Colony formation assay

The colony formation assay was performed in 6 well plates as we have previously described [20]. Briefly, ten days after plating, or when colonies of 30–50 cells were observed, colonies were either mock treated or treated with 5nM of paclitaxel continuously for 3 weeks by addition of paclitaxel to the feeder layer. Colony viability was assessed by phase contrast microscopy. Viable colonies appeared translucent and circular with regular borders. Viability was confirmed by isolation and mechanical dissociation of representative colonies in each condition followed by trypan blue staining.

## Statistical analysis

Results are reported as mean ± Standard Deviation of three or more independent experiments. Unless otherwise indicated, statistical significance of difference was assessed

by two-tailed Student's t using Prism (V.4 Graphpad, San Diego, CA) and Excel. The level of significance was set at $p<0.05$.

## Results

### UNC-45A overexpression correlates with paclitaxel resistance in ovarian cancer.

We and others have previously shown that UNC-45A overexpression correlates with patients' poor outcome in ovarian and breast cancer [9, 12]. For ovarian cancer in particular, a significant contributor to poor outcome is recurrence after developing chemoresistance to the MT stabilizing agent paclitaxel [21–25]. Thus, we set forth to determine whether UNC-45A overexpression is specifically associated to paclitaxel resistance in ovarian cancer. To this end, clinical specimens of ovarian cancer from patients that recurred and patients that did not recur were subjected to immunohistochemistry for UNC-45A. Specifically, ovarian cancer chemoresistance is defined as the pathologic or radiologic evidence of tumor recurrence within 6 months from complete treatment. We found that clinical specimens derived from recurrent and chemoresistant patients had significantly higher UNC-45A levels as compared to chemosensitive patients that did not recur. Representative staining for UNC-45A expression in non recurrent and recurrent cancers is given in Figure 1A. Quantification of staining intensity is given in Figure 1B. The specificity of the UNC-45A antibody for immunohistochemistry was validated using shRNA scramble and shRNA-UNC-45A in cancer cells (Supplementary Figure 1). To directly assess whether UNC-45A overexpression is specifically associated to paclitaxel chemoresistance, we generated matched pairs of paclitaxel-sensitive and paclitaxel-resistant cells by exposing COV362 ovarian cancer cells to either mock (vehicle), or their $IC_{50}$ concentration of paclitaxel for 3 cycles or continuously over a period of three weeks. At the end of the treatment, polyclonal cells were ~5 fold less sensitive to paclitaxel than vehicle treated cells, and clonal cells were between 15 and 20 fold less sensitive to paclitaxel than vehicle treated cells (Figure 1C). Importantly, chemoresistance was specific to paclitaxel, as sensitivity to a DNA-targeting chemotherapeutic agent, carboplatin, was not significantly different between these populations of cells (Figure 1D). To exclude the possibility that the difference in $IC_{50}$ values between the paclitaxel-sensitive and paclitaxel-resistant populations was the result of differential ability of paclitaxel to either enter or be retained by the cell, we measured the intracellular concentrations of the drug via HPLC. As shown in Figure 1E, intracellular concentrations of paclitaxel were not significantly different. Next, we measured the expression levels of UNC-45A in paclitaxel-sensitive and paclitaxel-resistant (polyclonal, and clones #1 and #7) ovarian cancer cells and found that paclitaxel-resistant cell lines expressed greater levels of UNC-45A than their paclitaxel-sensitive counterparts (Figure 1F). Next,we wanted to determine whether there was a correlation between intrinsic paclitaxel sensitivity and UNC-45A expression in a panel of ovarian cancer cell lines. To this end, UNC-45A levels and paclitaxel sensitivity were measured in Kuramochi, OVSAHO, JHOS2 and COV362 ovarian cancer cells. As shown in Figure 1G, cells with lower (< 5 nM) $IC_{50}$ to paclitaxel also had lower UNC-45A expression levels. Taken together, these data suggest that UNC-45A may be implicated in ovarian cancer cells' survival and resistance to the microtubule stabilizing agent paclitaxel.

### UNC-45A overexpressing cells resist chromosome missegregation and aneuploidy when treated with clinically relevant concentrations of paclitaxel.

Micromolar concentrations of paclitaxel kill mitotic cells by arresting them in the G2/M phase of the cell cycle (32–34). Recent evidence, however, indicates that clinically relevant concentrations of paclitaxel are in the low nanomolar range and cause chromosome missegregation on multipolar spindles resulting in aneuploidy, loss of essential chromosomal material and cell death (3, 4). Thus, we initially determined the fate of ovarian cancer cells exposed to clinically relevant concentrations of paclitaxel. To this end, COV362 ovarian cancer cells were mock treated or treated with 5, 10 or 30 nM paclitaxel and spindles per cell were counted following their visualization with α-tubulin antibody (Figure 2A). We found that cells treated with paclitaxel accumulated multipolar spindles in a concentration-dependent manner (Figure 2B). Next, we asked the question of whether UNC-45A overexpressing cells that are paclitaxel resistant, resist chromosome missegregation and aneuploidy following paclitaxel treatment. To this end, sensitive and paclitaxel-resistant (clone #7) COV362 cells were treated with clinically relevant concentrations of paclitaxel and the number of cells containing multipolar (>2) spindles were counted over time. As shown in Figure 2C, COV362 sensitive cells accumulated multipolar spindles over time while resistant cells kept dividing on bipolar spindles. To further confirm these results, sensitive and resistant cells were exposed to 5nM paclitaxel and the mixoploid profile (<2n and >4n) was evaluated by FACS analysis. As shown in Figure 2D, paclitaxel sensitive cells accumulate a mixoploid profile over time while paclitaxel-resistant cells remain nearly diploid. Quantification of percentage of cells containing a mixoploid profile per condition is given in Figure 2E. Similar results were obtained using paclitaxel-resistant polyclonal cells and clone #1 (Supplementary Figure 2). Taken together this suggests that paclitaxel resistance in UNC-45A overexpressing ovarian cancer cells could be due to UNC-45A antagonizing the effects of paclitaxel by decreasing MT stability and avoiding multipolar mitotic spindles (35).

### UNC-45A is a mitotic-spindle-associated protein whose depletion results with impaired mitotic progression.

We and others have previously shown that UNC-45A is overexpressed in human ovarian and breast cancers and that its loss results with reduced cell proliferation [9, 12]. In osteosarcoma and cervical cancer cells, UNC-45A has been recently shown to co-localize with γ-tubulin at the microtubule organizing center (MTOC) and to control cell proliferation via regulating centrosomes positioning during mitosis [14]. To gain further insight on the role of UNC-45A during cell division, we first asked whether, in addition to localization with γ-tubulin at the MTOC, UNC-45A could also co-localize with MTs during mitosis. To this end, we determined the subcellular localization of endogenous UNC-45A in both HeLa cancer cells and NIH3T3 fibroblasts during mitosis. As show in Figure 3, we found that UNC-45A co-localizes with mitotic microtubules throughout cell division from prophase to telophase in both cancer cells (A) and fibroblasts (B). The same co-localization of UNC-45A with the mitotic spindle was found in COV362 ovarian cancer cells Figure 3C. The specificity of the UNC-45A antibody used in immunofluorescence experiments is given in Supplementary Figure 3. Since mitotic spindles regulate cell division and because loss of

UNC-45A has been shown to hinder cell proliferation in several human cancer cells, we evaluated the effect of UNC-45A depletion on mitotic progression.

To this end, UNC-45A was knocked down via lentiviral-mediated delivery of scramble or UNC-45A shRNA in HeLa cells and the efficiency of the knock down was evaluated with Western blot analysis. As shown in Figure 3D, we obtained approximately 80% of protein knockdown. Scramble and UNC-45A knockdown cells were stained for DAPI and analyzed for their mitotic index and for the percentage of metaphase versus mitotic cells (Figure 3E). Loss of UNC-45A resulted with almost double the mitotic index (Figure 3F) and almost a 30% increase in the percentage of metaphase cells over mitotic cells (Figure 3G). Similar results were obtained using a second shRNA-UNC-45A (KD#2) and are shown in Supplementary Figure 4A and B. Taken together this suggests that UNC-45A is a novel mitotic spindle-associated protein which plays a crucial role during mitotic progression in both cancer and fibroblasts cells.

### Loss of UNC-45A results with mitotic defects consistent with overly stable MTs.

The effect of UNC-45A loss on mitotic index and progression together with its localization with mitotic spindle suggests that UNC-45A may be a key regulator of spindle-associated functions. In this scenario, loss of UNC-45A would result with defects during chromosome congression and segregation [26, 27]. To determine the effects of UNC-45A loss on chromosome congression, we measured pole to pole distance and metaphase plate width in scramble and UNC-45A knockdown HeLa cells subjected to γ-tubulin and DAPI staining (Figure 4A). As shown in Figure 4B, loss of UNC-45A resulted with approximately 50% increase in the distance between centrosomes as compared to control. Loss of UNC-45A also resulted with almost double the metaphase plate width (Figure 4C) as compared to control. To determine the effects of UNC-45A loss on chromosome alignment, scramble and UNC-45A knockdown HeLa cells were stained with DAPI (Figure 4D) and the effects of UNC-45A depletion on chromosome alignment was evaluated by counting the number of cells whose chromosomes were clearly separated from the metaphase plate. As shown in Figure 4E, loss of UNC-45A resulted with a threefold increase in the percentage of cells that had misaligned chromosomes as compared to control. To determine the effects of UNC-45A loss on chromosome segregation, scramble and UNC-45A knockdown HeLa cells were stained with DAPI (Figure 4F) and the effect of UNC-45A depletion on segregation was evaluated by counting the number of cells whose chromosomes trailed behind newly separated DNA in anaphase. As shown in Figure 4G, loss of UNC-45A resulted with nearly three times the percentage of cells having lagging chromosomes as compared to controls. Importantly, loss of UNC-45A also resulted with an increase in the number of cells having multipolar spindles (Figure 4H). Specifically, the percentage of metaphase HeLa cells having multipolar spindles in the UNC-45A knockdown condition was fourfold as compared to controls (Figure 4I). Similar results were obtained using a second shRNA-UNC-45A (KD#2) and are shown in Supplementary Figure 4C, D and E. Importantly, we found that UNC-45A overexpressing clinical specimens (from recurrent and chemoresistant patients) have less mitotic abnormalities as compared to specimens derived from patients that are non-recurrent (Figure 4J and K. This is consistent with a role for UNC-45A in counteracting the paclitaxel effects on MTs *in vivo.*

Taken together the loss of UNC-45A caused a phenotype that is similar to the one caused by clinically relevant doses of paclitaxel in cancer cells [26, 27] which is consistent with hyper-stabilization of mitotic spindles.

### UNC-45A is a microtubule destabilizing protein.

Because in cells the loss of UNC-45A results with a phenotype consistent with excessive mitotic spindle stabilization, we set forth to determine MT stability of spindles in scramble and UNC-45A knockdown cells. To this end, HeLa cancer cells (Figure 5A) or NIHT3T3 fibroblasts (Figure 5B) were transduced with either scramble or UNC-45A shRNA and the MT stability was evaluated following staining for acetylated α-tubulin. Importantly, acetylation a is MT post-translational modification associated with long-lived MTs and therefore is used as a marker for stable and long-lived MTs [28]. Quantification of florescence intensity in each condition reveled that loss of UNC-45A resulted with nearly a twofold increase in spindle stability for both cancer cells (Figure 5C) and fibroblasts (Figure 5D) suggesting that the loss of UNC-45A may act as a MT destabilizing protein and its loss results with excessive MT stabilization. Complementary experiments of UNC-45A overexpression revealed that an increase in UNC-45A expression is associated with significant reduction in the levels of acetylated alpha-tubulin, here used as a marker of spindle stability (Supplementary Figure 5).

To directly test whether UNC-45A modulates MT stability and whether UNC-45A binds MTs in the absence of any other cellular factors, we used TIRF microscopy to evaluate the binding of purified UNC-45A-GFP (Supplementary Figure 6) to paclitaxel-stabilized, rhodamine-labeled bovine-brain microtubules (Figure 5E). We observed robust binding of green UNC-45A-GFP to the red microtubules (Figure 5F), suggesting that UNC45A binds microtubules directly, without the requirement for any additional cellular factors. To determine whether UNC-45A acted to destabilize paclitaxel-stabilized MTs in our cell-free system, we collected time-lapse movies of paclitaxel-stabilized MTs, in the presence and absence of UNC-45A-GFP. We found that while taxol-stabilized microtubules in the control movies without UNC-45A-GFP showed little or no depolymerization over 60 minutes of collecting data, addition of UNC-45A-GFP to the imaging chamber resulted in depolymerization of the microtubule over time (Figure 5G). Because it appeared that higher concentrations of UNC-45A-GFP led to more rapid microtubule depolymerization, we quantified the average microtubule depolymerization rate for increasing concentrations of UNC-45A-GFP. We found that 0.6 μM of UNC-45-GFP depolymerized microtubules ~5-fold faster than the controls, and 1.2 μM of UNC-45A-GFP depolymerized microtubule ends ~10-fold faster than the controls (Figure 5H). Next, we determined whether endogenous UNC-45A binds to MTs in living cells. To this end, lysates from COV362 cells were either mock treated or treated with 1 μM of taxol for 1 hour, and polymerized tubulin and associated proteins were separated in pellet and supernatant fractions via ultracentrifugation. As shown in Figure 5I, after taxol treatment and tubulin polymerization, both UNC-45A and tubulin were found in the pellet fractions. Quantification of the percentage of UNC-45A bound to MTs shows that nearly 100% of UNC-45A is bound to the available polymerized MTs (Figure 5J). Importantly while UNC-45A was found to immunoprecipitate with Hsp90 (here used as an immunoprecipitation positive control [29] it did not precipitate with alpha-

tubulin (Figure 5K) suggesting that *in vivo* UNC-45A preferentially binds to polymerized MTs. Taken together this strongly suggests that UNC-45A is a MT destabilizing protein that directly destabilizes microtubules in living cells and *in vitro.*

## UNC-45A depletion exacerbates paclitaxel-mediated stabilizing effects on mitotic spindles and increases sensitivity to paclitaxel.

Our data indicate that UNC-45A overexpressing ovarian cancer cells resist cell death when exposed to the MT stabilizing agent paclitaxel. Our data also indicate that UNC-45A is a MT-associated protein that acts as a MTs destabilizer in cells and *in vitro*. Thus, we asked the question of whether UNC-45A overexpressing, paclitaxel-resistant cells, are characterized by endogenously less stable MTs. To this end, we measured the expression levels of acetylated-tubulin in paclitaxel-sensitive and paclitaxel-resistant (polyclonal, and clones #1 and #7) ovarian cancer cells and found that UNC-45A overexpression and paclitaxel chemoresistance was associated with reduction in MT stability as determined by Western blot analysis (Figure 6A). To confirm that this was due to UNC-45A, we performed complementary experiments of UNC-45A knockdown and overexpression in COV362 ovarian cancer cells and showed that reduction of UNC-45A expression results with approximate 80% increase in acetylated-tubulin expression levels (Figure 6B, *left*) while UNC-45A overexpression results with an over 60% decrease of acetylated tubulin expression levels (Figure 6B, *right*). Next asked the question on whether loss of UNC-45A would result with increased cancer cell sensitivity to paclitaxel. To this end, we first tested the effect of drug treatment on incidence of cells containing multipolar spindles in presence and in absence of UNC-45A. As shown in Figure 6C and D, paclitaxel treatment following UNC-45A knockdown and γ-tubulin and DAPI staining resulted with a significantly higher percentage of cells containing multipolar spindles as compared to controls. Complementary experiments of UNC-45A overexpression (Figure 6E and F) shows that overexpressing UNC-45A cells remain mostly bipolar when exposed to increasing concentration of paclitaxel. This suggests that, similarly to paclitaxel, loss of UNC-45A stabilizes MTs predisposing cancer cells to chromosome missegregation on multipolar spindles. Thus, we next we tested whether depletion of UNC-45A would increase cancer cells' sensitivity to paclitaxel by exacerbating its effects on mitotic spindles. To this end, we measured the residual cell viability of scramble and UNC-45A knockdown COV362 ovarian cancer cells exposed to 5nM paclitaxel over a period of 6 days. As shown in Figure 6G, depletion of UNC-45A increased cells' sensitivity to paclitaxel as compared to the control counterpart. Because tumors *in vivo* are tridimensional, we next evaluated the effect of UNC-45A loss on paclitaxel sensitivity in cancer cells grown as tridimensional structures. For these experiments we used SKOV-3 ovarian cancer cells because they are known to form spheroids [30]. Specifically, UNC-45A was knocked down in SKOV-3 ovarian cancer cells (Supplementary Figure 7A) and scramble and UNC-45A knockdown cells were grown in soft agar for 10 days prior being exposed to 5nM paclitaxel over a period of three weeks. At the end of this period, colonies in each condition were biopsied and cell viability was evaluated via trypan-blue exclusion assay. As shown in Figure 6H, UNC-45A depletion resulted with smaller colonies of cells that were significantly more sensitive to paclitaxel treatment as compared to control cells. Quantification of viable versus nonviable colonies in each condition is given in Figure 6I. Because we and others have previously shown that loss

of UNC-45A can affect proliferation rate in some cancer cells [9, 12], we measured the daily proliferation rate of shRNA scramble and shRNA-UNC-45A COV362 and SKOV-3 cells. As shown in Supplementary Figure 7B, reduction of UNC-45A levels resulted in a mild, yet significant decrease in cells' proliferation rate in both COV362 (*left panel*) and SKOV-3 (*right panel*) cells. In this context, the increased sensitivity to paclitaxel in UNC-45A knockdown cells is particularly striking considering that paclitaxel targets rapidly dividing cells.

Because our data show that UNC-45A is a novel MT destabilizing protein, we tested whether the loss of one of the most well known MT destabilizing proteins, MCAK, would cause similar effects in terms of increasing paclitaxel sensitivity in ovarian cancer cells. For this, control siRNA and siMCAK treated COV362 cells were subjected to Western blot analysis for MCAK and acetylated tubulin expression. As shown in Figure 6J and consistent with its effect as a MT destabilizing protein, a less than 50% reduction in MCAK expression resulted in an almost two-fold increase in the levels of acetylated tubulin, here used as a marker of MT stability. Importantly, further reduction of MCAK expression levels resulted with severe cell toxicity and death (data not shown). Next, siRNA scramble and siRNA-MCAK treated cells were exposed to 5nM paclitaxel and residual cell viability was measured over a period of three days. As shown in Figure 6K, partial loss of MCAK resulted with increased cells' sensitivity to paclitaxel as compared to the control counterpart. While UNC-45A knockdown in SKOV-3 cells did not result in reduction in the levels of the well known MT destabilizing protein MCAK, (Supplementary Figure 9A), it was accompanied by an increase in the acetylation levels of alpha-tubulin (Supplementary Figure 9A) and in increase in mitotic index and cells containing multipolar spindles (Supplementary Figure 9B, *left and right* respectively). Taken together, this suggests that UNC-45A plays a direct role in modulating ovarian cancer cells' sensitivity to paclitaxel, its depletion restores cancer cells' sensitivity to the drug, and the effect is mediated by perturbation of MT stability (Figure 7).

## Discussion

The results of this study demonstrate that UNC-45A is a mitotic-spindle-associated protein which acts as a regulator of mitotic progression via destabilizing MTs *in vitro* and *in vivo* in human cells. Our data also demonstrate that human cancer cells resistant to the MT stabilizer paclitaxel upregulate UNC-45A and that the abnormally hypo-stable MT levels conferred by UNC-45A to cancer cells allow them to escape the otherwise lethal effect of paclitaxel. Most importantly, we demonstrate that depletion of UNC-45A increases human cancer cell sensitivity to paclitaxel by exacerbating its mitotic spindle hyper-stabilizing effects.

A number of studies, including studies from our laboratory, have revealed that in human cancer cells, UNC-45A is a NMII binding and co-localizing protein that plays a role in regulation of NMII folding, activity and binding to actin [7–10, 12]. Furthermore, we recently proposed that in neurons, UNC-45A is required for neurite extension [11]. In this scenario, UNC-45A acts like an inhibitor of NMII activation and its loss increases NMII contractility and F-actin retrograde flow at the growth cone [11, 31–33]. Independent of NMII regulation, UNC-45A has been shown to be a modulator of progesterone receptor/

Hsp90 complex [13] and a centromosomal-associated protein in human cancer cells[14]. Notably, one of the most well-known cell cycle regulators, the cyclin-dependent kinase inhibitor 1B (p27) is both a MT- and NMII-associated protein and has been shown to regulate both NMII activity and MT stability in normal and cancer cells [31–37].

Here we show that UNC-45A is a novel microtubule- and spindle-associated protein with MT destabilizing effects *in vivo*. Mechanistically we show that UNC-45A binds directly to paclitaxel-stabilized MTs in absence of any other cellular component and that it depolymerizes paclitaxel-stabilized MTs in a concentration-dependent manner, thus identifying UNC-45A a novel MT depolymerase. Unlike many of the so far identified MTs depolymerizing or severing proteins, UNC-45A does not have an identified ATP-ase domain and has activity in absence of ATP [38–40]. This suggests that UNC-45A-mediated MT destabilization is ATP-independent, and puts UNC-45A in a unique class of MT destabilizing proteins.

Here we also show that ovarian cancer patients that have developed chemoresistance to paclitaxel present with significantly higher levels of UNC-45A in their tumors as compared to patients that are sensitive to the drug. This holds true for matched-pairs of paclitaxel sensitive and paclitaxel resistant ovarian cancer cells that were originated in the laboratory via exposure to paclitaxel over the period of several weeks. In these cells, paclitaxel, but not carboplatin resistance, is associated with higher UNC-45A levels. Importantly, the different sensitivity to paclitaxel was not due to differences in intracellular levels of the drug. This suggests that UNC-45A confers a selective survival advantage to cancer cells following paclitaxel exposure.

The role of paclitaxel in stabilizing MTs is well established. The effect of paclitaxel-mediated stabilization on cancer cells' cell cycle and ultimately cell death is less clear. High doses (in the micromolar range) of paclitaxel have been shown to stabilize MTs and kill cancer cells by causing a mitotic arrest in G2 phase of the cell cycle [26, 41, 42]. On the other hand, lower doses (in the nanomolar range) of paclitaxel have been proposed to stabilize MTs and kill cancer cells due to chromosome missegregation on multipolar spindles [43, 44]. Importantly, because paclitaxel is known to accumulate in cancer cells *in vitro* and *in vivo* (intratumorally, in patients), it has been recently proposed that therapeutically relevant concentrations of paclitaxel are in the nanomolar range [24, 45].

Here we show that ovarian cancer cells die in a dose-dependent manner when exposed to therapeutically relevant concentrations of paclitaxel, and that cell death following treatment is preceded by the appearance of cells with multipolar spindles. This is consistent with what has been shown in breast cancer cells *in vitro* and in tumor samples *in vivo* [45]. Because supernumerary centrosomes can lead to multipolar spindles [46], it has been proposed that an increase in MT stability via either loss of MT destabilizing proteins or treatment with MT stabilizing agent, can lead to abnormal spindle pole formation, supernumerary centrosomes and aneuploidy [27, 44, 47]. We also show that paclitaxel-resistant, UNC-45A overexpressing ovarian cancer cells maintain bipolar spindles and diploidy when exposed to paclitaxel. Furthermore, genetic silencing of UNC-45A restores cancer cells' sensitivity to paclitaxel via a mechanism that is consistent with exacerbation of the morphological defects

caused by paclitaxel on spindle MTs. This is consistent with what is observed in cancer cells following combination of anti-MT agents and kinesins [48]. Importantly, additional MT destabilizing proteins including the spleen tyrosine kinase (SYK) [49] pathways have been shown to be aberrantly expressed in cancer cells resistant to paclitaxel and SYK's pharmacological inhibition has been shown to restore cancer cells' sensitivity to mitotic poisons.

To conclude, our results put UNC-45A as a key protein involved in regulating cell cycle, mitotic progression, MT stability and human cancer behavior with regard to chemotherapy.

## Supplementary Material

Refer to Web version on PubMed Central for supplementary material.

## Acknowledgments

We are grateful to Dr. Henry Epstein (1944–2013) for his friendship and helpful discussions and to Dr. David Odde for providing with helpful insights. We thank Guillermo Marques (University of Minnesota Imaging Center) for assistance with image analysis. This work was supported by Department of Defense Ovarian Cancer Research Program Grant OC160377, the Minnesota Ovarian Cancer Alliance and the Randy Shaver Cancer Research Funds to Martina Bazzaro. Melissa Gardner was supported by NIH grant NIGMS R01 GM-103833. Ashley Mooneyham was funded by the NIH T32 CA009138 training grant. The funders had no role in study design, data collection and analysis, decision to publish or preparation of the manuscript. The authors declare no conflict of interests.

## References

[1]. Barral JM, Bauer CC, Ortiz I, Epstein HF, Unc-45 mutations in Caenorhabditis elegans implicate a CRO1/She4p-like domain in myosin assembly, The Journal of cell biology, 143 (1998) 1215–1225. [PubMed: 9832550]

[2]. Price MG, Landsverk ML, Barral JM, Epstein HF, Two mammalian UNC-45 isoforms are related to distinct cytoskeletal and muscle-specific functions, Journal of cell science, 115 (2002) 4013–4023. [PubMed: 12356907]

[3]. Barral JM, Hutagalung AH, Brinker A, Hartl FU, Epstein HF, Role of the myosin assembly protein UNC-45 as a molecular chaperone for myosin, Science, 295 (2002) 669–671. [PubMed: 11809970]

[4]. Lee CF, Melkani GC, Bernstein SI, The UNC-45 myosin chaperone: from worms to flies to vertebrates, International review of cell and molecular biology, 313 (2014) 103–144. [PubMed: 25376491]

[5]. Ni W, Odunuga OO, UCS proteins: chaperones for myosin and co-chaperones for Hsp90, Sub-cellular biochemistry, 78 (2015) 133–152. [PubMed: 25487020]

[6]. Bird JE, Takagi Y, Billington N, Strub MP, Sellers JR, Friedman TB, Chaperone-enhanced purification of unconventional myosin 15, a molecular motor specialized for stereocilia protein trafficking, Proceedings of the National Academy of Sciences of the United States of America, 111 (2014) 12390–12395. [PubMed: 25114250]

[7]. Shi H, Blobel G, UNC-45/CRO1/She4p (UCS) protein forms elongated dimer and joins two myosin heads near their actin binding region, Proceedings of the National Academy of Sciences of the United States of America, 107 (2010) 21382–21387. [PubMed: 21115842]

[8]. Lehtimaki JI, Fenix AM, Kotila TM, Balistreri G, Paavolainen L, Varjosalo M, Burnette DT, Lappalainen P, UNC-45a promotes myosin folding and stress fiber assembly, The Journal of cell biology, (2017).

[9]. Bazzaro M, Santillan A, Lin Z, Tang T, Lee MK, Bristow RE, Shih Ie M, Roden RB, Myosin II co-chaperone general cell UNC-45 overexpression is associated with ovarian cancer, rapid proliferation, and motility, Am J Pathol, 171 (2007) 1640–1649. [PubMed: 17872978]

[10]. Iizuka Y, Cichocki F, Sieben A, Sforza F, Karim R, Coughlin K, Isaksson Vogel R, Gavioli R, McCullar V, Lenvik T, Lee M, Miller J, Bazzaro M, UNC-45A Is a Nonmuscle Myosin IIA Chaperone Required for NK Cell Cytotoxicity via Control of Lytic Granule Secretion, J Immunol, 195 (2015) 4760–4770. [PubMed: 26438524]

[11]. Iizuka Y, Mooneyham A, Sieben A, Chen K, Maile M, Hellweg R, Schutz F, Teckle K, Starr T, Thayanithy V, Vogel RI, Lou E, Lee MK, Bazzaro M, UNC-45A is required for neurite extension via controlling NMII activation, Mol Biol Cell, 28 (2017) 1337–1346. [PubMed: 28356421]

[12]. Guo W, Chen D, Fan Z, Epstein HF, Differential turnover of myosin chaperone UNC-45A isoforms increases in metastatic human breast cancer, Journal of molecular biology, 412 (2011) 365–378. [PubMed: 21802425]

[13]. Chadli A, Graham JD, Abel MG, Jackson TA, Gordon DF, Wood WM, Felts SJ, Horwitz KB, Toft D, GCUNC-45 is a novel regulator for the progesterone receptor/hsp90 chaperoning pathway, Molecular and cellular biology, 26 (2006) 1722–1730. [PubMed: 16478993]

[14]. Jilani Y, Lu S, Lei H, Karnitz LM, Chadli A, UNC45A localizes to centrosomes and regulates cancer cell proliferation through ChK1 activation, Cancer Lett, 357 (2015) 114–120. [PubMed: 25444911]

[15]. Greenlee RT, Hill-Harmon MB, Murray T, Thun M, Cancer statistics, 2001, CA: a cancer journal for clinicians, 51 (2001) 15–36. [PubMed: 11577478]

[16]. Agarwal R, Kaye SB, Ovarian cancer: strategies for overcoming resistance to chemotherapy, Nature reviews. Cancer, 3 (2003) 502–516. [PubMed: 12835670]

[17]. Coombes C, Yamamoto A, McClellan M, Reid TA, Plooster M, Luxton GW, Alper J, Howard J, Gardner MK, Mechanism of microtubule lumen entry for the alpha-tubulin acetyltransferase enzyme alphaTAT1, Proceedings of the National Academy of Sciences of the United States of America, 113 (2016) E7176–E7184. [PubMed: 27803321]

[18]. Reid TA, Schuster BM, Mann BJ, Balchand SK, Plooster M, McClellan M, Coombes CE, Wadsworth P, Gardner MK, Suppression of microtubule assembly kinetics by the mitotic protein TPX2, Journal of cell science, 129 (2016) 1319–1328. [PubMed: 26869224]

[19]. Coughlin K, Anchoori R, Iizuka Y, Meints J, MacNeill L, Vogel RI, Orlowski RZ, Lee MK, Roden RB, Bazzaro M, Small-molecule RA-9 inhibits proteasome-associated DUBs and ovarian cancer in vitro and in vivo via exacerbating unfolded protein responses, Clin Cancer Res, 20 (2014) 3174–3186. [PubMed: 24727327]

[20]. Anchoori RK, Khan SR, Sueblinvong T, Felthauser A, Iizuka Y, Gavioli R, Destro F, Isaksson Vogel R, Peng S, Roden RB, Bazzaro M, Stressing the ubiquitin-proteasome system without 20S proteolytic inhibition selectively kills cervical cancer cells, PLoS One, 6 (2011) e23888. [PubMed: 21909374]

[21]. Einzig AI, Wiernik PH, Sasloff J, Runowicz CD, Goldberg GL, Phase II study and long-term follow-up of patients treated with taxol for advanced ovarian adenocarcinoma, Journal of clinical oncology : official journal of the American Society of Clinical Oncology, 10 (1992) 1748–1753. [PubMed: 1357110]

[22]. Wiernik PH, Schwartz EL, Strauman JJ, Dutcher JP, Lipton RB, Paietta E, Phase I clinical and pharmacokinetic study of taxol, Cancer research, 47 (1987) 2486–2493. [PubMed: 2882837]

[23]. Amos LA, Lowe J, How Taxol stabilises microtubule structure, Chemistry & biology, 6 (1999) R65–69. [PubMed: 10074470]

[24]. Weaver BA, How Taxol/paclitaxel kills cancer cells, Molecular biology of the cell, 25 (2014) 2677–2681. [PubMed: 25213191]

[25]. N.C.C. Network, NCCN Clinical Practice Guidelines for Ovarian Cancer, in: N.C.P.G.i. Oncology (Ed.), 2015.

[26]. Jordan MA, Toso RJ, Thrower D, Wilson L, Mechanism of mitotic block and inhibition of cell proliferation by taxol at low concentrations, Proceedings of the National Academy of Sciences of the United States of America, 90 (1993) 9552–9556. [PubMed: 8105478]

[27]. Yvon AM, Wadsworth P, Jordan MA, Taxol suppresses dynamics of individual microtubules in living human tumor cells, Mol Biol Cell, 10 (1999) 947–959. [PubMed: 10198049]

[28]. Janke C, Montagnac G, Causes and Consequences of Microtubule Acetylation, Curr Biol, 27 (2017) R1287–R1292. [PubMed: 29207274]

[29]. Liu L, Srikakulam R, Winkelmann DA, Unc45 activates Hsp90-dependent folding of the myosin motor domain, J Biol Chem, 283 (2008) 13185–13193. [PubMed: 18326487]

[30]. Raghavan S, Ward MR, Rowley KR, Wold RM, Takayama S, Buckanovich RJ, Mehta G, Formation of stable small cell number three-dimensional ovarian cancer spheroids using hanging drop arrays for preclinical drug sensitivity assays, Gynecol Oncol, 138 (2015) 181–189. [PubMed: 25913133]

[31]. Besson A, Gurian-West M, Schmidt A, Hall A, Roberts JM, p27Kip1 modulates cell migration through the regulation of RhoA activation, Genes & development, 18 (2004) 862–876. [PubMed: 15078817]

[32]. Godin JD, Thomas N, Laguesse S, Malinouskaya L, Close P, Malaise O, Purnelle A, Raineteau O, Campbell K, Fero M, Moonen G, Malgrange B, Chariot A, Metin C, Besson A, Nguyen L, p27(Kip1) is a microtubule-associated protein that promotes microtubule polymerization during neuron migration, Developmental cell, 23 (2012) 729–744. [PubMed: 23022035]

[33]. Serres MP, Kossatz U, Chi Y, Roberts JM, Malek NP, Besson A, p27(Kip1) controls cytokinesis via the regulation of citron kinase activation, The Journal of clinical investigation, 122 (2012) 844–858. [PubMed: 22293177]

[34]. Fabris L, Berton S, Pellizzari I, Segatto I, D'Andrea S, Armenia J, Bomben R, Schiappacassi M, Gattei V, Philips MR, Vecchione A, Belletti B, Baldassarre G, p27kip1 controls H-Ras/MAPK activation and cell cycle entry via modulation of MT stability, Proceedings of the National Academy of Sciences of the United States of America, 112 (2015) 13916–13921. [PubMed: 26512117]

[35]. Baldassarre G, Belletti B, Nicoloso MS, Schiappacassi M, Vecchione A, Spessotto P, Morrione A, Canzonieri V, Colombatti A, p27(Kip1)-stathmin interaction influences sarcoma cell migration and invasion, Cancer cell, 7 (2005) 51–63. [PubMed: 15652749]

[36]. Murthy K, Wadsworth P, Myosin-II-dependent localization and dynamics of F-actin during cytokinesis, Current biology : CB, 15 (2005) 724–731. [PubMed: 15854904]

[37]. Bezanilla M, Wilson JM, Pollard TD, Fission yeast myosin-II isoforms assemble into contractile rings at distinct times during mitosis, Current biology : CB, 10 (2000) 397–400. [PubMed: 10753748]

[38]. Sharp DJ, Ross JL, Microtubule-severing enzymes at the cutting edge, Journal of cell science, 125 (2012) 2561–2569. [PubMed: 22595526]

[39]. Roll-Mecak A, McNally FJ, Microtubule-severing enzymes, Current opinion in cell biology, 22 (2010) 96–103. [PubMed: 19963362]

[40]. Walczak CE, Gayek S, Ohi R, Microtubule-depolymerizing kinesins, Annual review of cell and developmental biology, 29 (2013) 417–441.

[41]. Schiff PB, Fant J, Horwitz SB, Promotion of microtubule assembly in vitro by taxol, Nature, 277 (1979) 665–667. [PubMed: 423966]

[42]. Schiff PB, Horwitz SB, Taxol stabilizes microtubules in mouse fibroblast cells, Proceedings of the National Academy of Sciences of the United States of America, 77 (1980) 1561–1565. [PubMed: 6103535]

[43]. Chen JG, Horwitz SB, Differential mitotic responses to microtubule-stabilizing and -destabilizing drugs, Cancer research, 62 (2002) 1935–1938. [PubMed: 11929805]

[44]. Hornick JE, Bader JR, Tribble EK, Trimble K, Breunig JS, Halpin ES, Vaughan KT, Hinchcliffe EH, Live-cell analysis of mitotic spindle formation in taxol-treated cells, Cell Motil Cytoskeleton, 65 (2008) 595–613. [PubMed: 18481305]

[45]. Zasadil LM, Andersen KA, Yeum D, Rocque GB, Wilke LG, Tevaarwerk AJ, Raines RT, Burkard ME, Weaver BA, Cytotoxicity of paclitaxel in breast cancer is due to chromosome missegregation on multipolar spindles, Science translational medicine, 6 (2014) 229ra243.

[46]. Maiato H, Logarinho E, Mitotic spindle multipolarity without centrosome amplification, Nat Cell Biol, 16 (2014) 386–394. [PubMed: 24914434]

[47]. Hu WF, Pomp O, Ben-Omran T, Kodani A, Henke K, Mochida GH, Yu TW, Woodworth MB, Bonnard C, Raj GS, Tan TT, Hamamy H, Masri A, Shboul M, Al Saffar M, Partlow JN, Al-Dosari M, Alazami A, Alowain M, Alkuraya FS, Reiter JF, Harris MP, Reversade B, Walsh CA,

Katanin p80 regulates human cortical development by limiting centriole and cilia number, Neuron, 84 (2014) 1240–1257. [PubMed: 25521379]

[48]. Hedrick DG, Stout JR, Walczak CE, Effects of anti-microtubule agents on microtubule organization in cells lacking the kinesin-13 MCAK, Cell cycle, 7 (2008) 2146–2156. [PubMed: 18635958]

[49]. Yu Y, Gaillard S, Phillip JM, Huang TC, Pinto SM, Tessarollo NG, Zhang Z, Pandey A, Wirtz D, Ayhan A, Davidson B, Wang TL, Shih Ie M, Inhibition of Spleen Tyrosine Kinase Potentiates Paclitaxel-Induced Cytotoxicity in Ovarian Cancer Cells by Stabilizing Microtubules, Cancer Cell, 28 (2015) 82–96. [PubMed: 26096845]

**Implications:**

These findings reveal novel and significant roles for UNC-45A in regulation of cytoskeletal dynamics, broadening our understanding of the basic mechanisms regulating microtubule stability and human cancer susceptibility to paclitaxel, one of the most widely used chemotherapy agents for the treatment of human cancers.

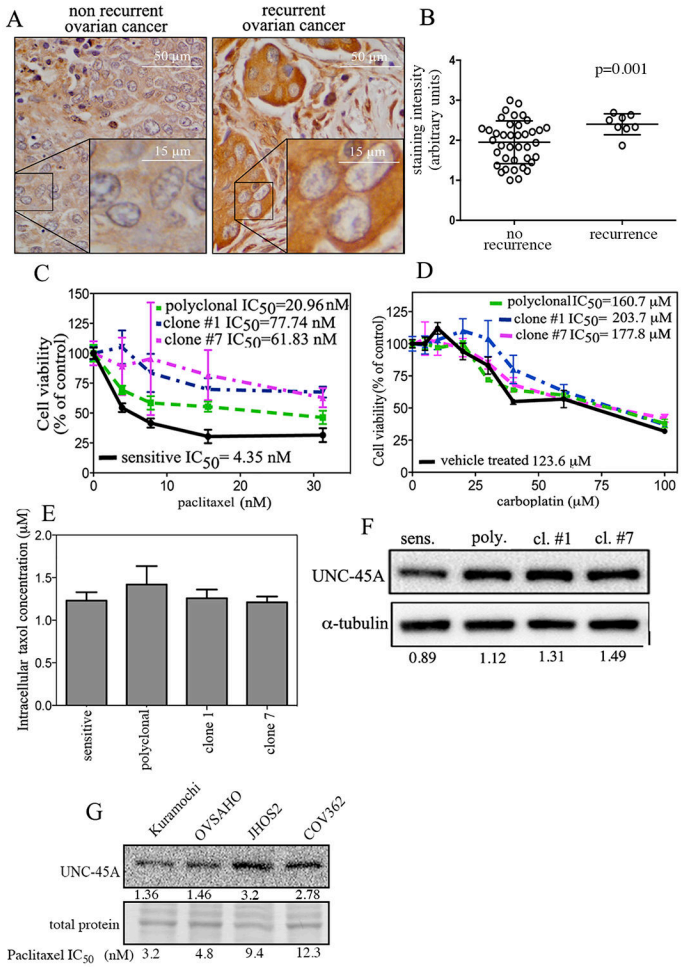


**Figure 1. UNC-45A is overexpressed in paclitaxel chemoresistant ovarian cancer.**

**A.** Immunohistochemical staining of UNC-45A in clinical specimens from patients with non recurrent (n=40) or recurrent (n=8) ovarian cancer. Representative examples of weak (*left*) and intense (*right*) UNC-45A staining. **B,** staining intensity for each case was graded as 0 (no staining), 1 (weak staining), 2 (moderate staining), and 3 (intense staining). **C**. Dose-dependent inhibition of cell viability of COV362 sensitive, polyclonal, clone #1, and clone #7 cells exposed to the indicated concentrations of paclitaxel over a period of 96 hours. **D.** Dose-dependent inhibition of cell viability of COV362 sensitive, polyclonal, clone #1, and clone #7 exposed to the indicated concentrations of carboplatin over a period of 48 hours. **E.** Intracellular concentrations of paclitaxel as measured via HPLC in lysates of sensitive and resistant COV362 cells pretreated with 100 nM paclitaxel. **F.** UNC-45A expression levels in sensitive, polyclonal, clone #1, and clone #7 COV362 ovarian cancer cells. Numbers indicate the ratio between UNC-45A and α-tubulin. All experiments were performed in triplicates. **G.** Expression levels of UNC-45A in ovarian cancer cell lines with different degrees of paclitaxel sensitivity as measured by WST assay following 48 hours drug exposure and expressed as $IC_{50}$. Numbers indicate the ratio between UNC-45A levels and total protein which was used as an equal loading control.

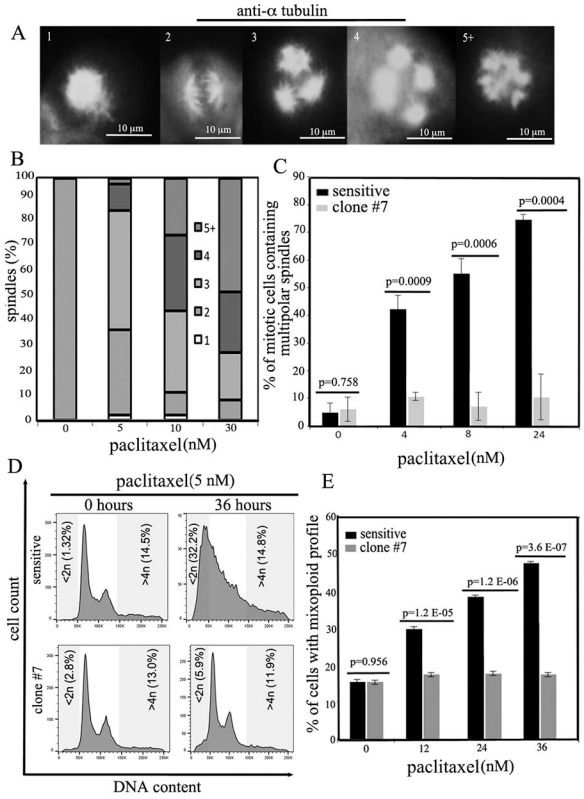


**Figure 2. Paclitaxel-resistant ovarian cancer cells overcome cell death on multipolar spindles.**

**A**. Mitotic figures containing multipolar spindles in COV362 ovarian cancer cells treated with clinically relevant concentrations of paclitaxel as evaluated by α-tubulin and DAPI staining. **B.** Dose-dependent formation of supernumerary spindle poles in paclitaxel treated cells. **C.** Following exposure to clinically relevant concentrations of paclitaxel (5nM), COV362 sensitive cells accumulate multipolar spindles over time while paclitaxel-resistant cells (clone #7) keep dividing on bipolar spindles. **D.** Paclitaxel-sensitive COV362 cells treated with clinically relevant concentrations of paclitaxel (5nM) accumulate mixoploid profile (<2n and >4n) over time while paclitaxel-resistant cells (clone 7) remain nearly diploid. **E**. Percentage of cells with mixoploid profile.

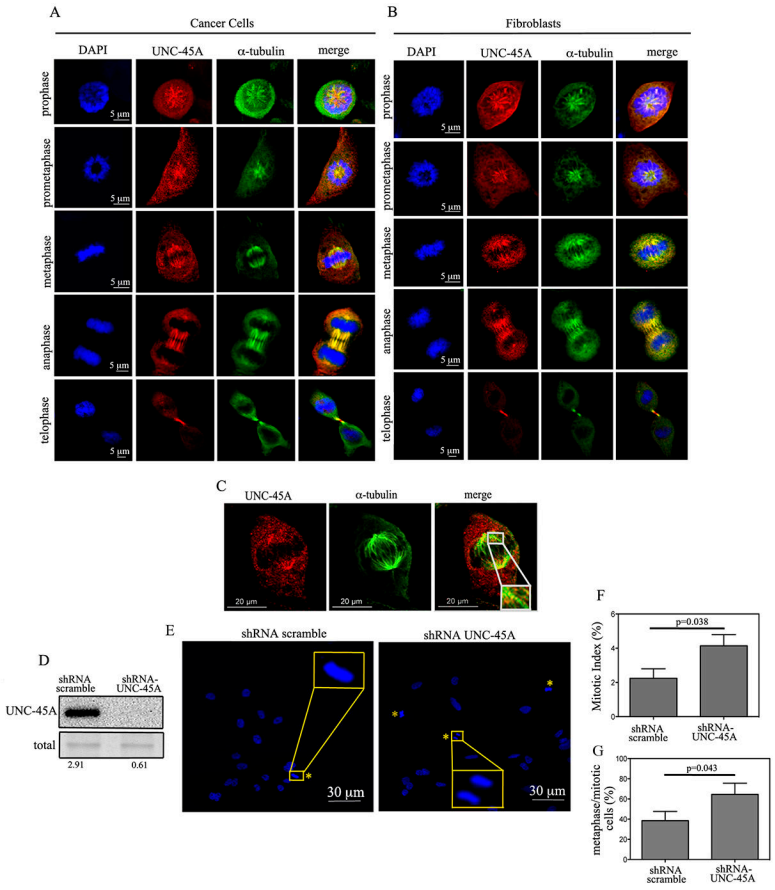


**Figure 3. UNC-45A is a spindle-associated protein that controls mitotic progression.**

(**A** and **B**). Shown are representative images of HeLa cancer cells (**A**) or NIH 3T3 fibroblasts (**B**) stained for UNC-45A (red), α-tubulin (green) and DNA (blue). **C.** Representative picture of metaphase COV362 ovarian cancer cell line stained for UNC-45A (red) and α-tubulin (green). Insert is a magnification showing co-localization. **D.** Western blot analysis for levels of UNC-45A in HeLa cells transduced with either shRNA scramble or shRNA-UNC-45A. Numbers indicate the ratio between UNC-45A and total protein. **E**. Representative images of mitotic HeLa cells (yellow asterisk) transfected with scramble or UNC-45A shRNAs. **F**. Mitotic index in shRNA scramble (n= 798) versus shRNA-UNC-45A (n=852) transduced HeLa cells. **G**. Percentage of metaphase over mitotic cells in shRNA scramble (n=24) versus shRNA-UNC-45A (n=31) transduced HeLa cells.

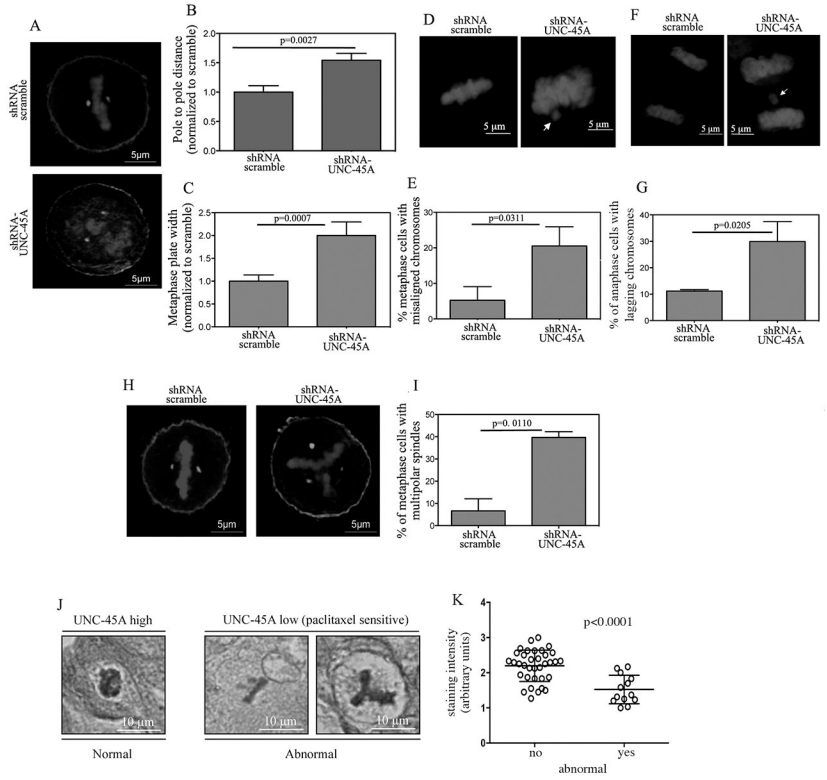


**Figure 4. Depletion of UNC-45A causes mitotic defects consistent with overly stable mitotic spindles.**

**A.** Representative images of HeLa cells transduced with either scramble or UNC-45A shRNAs and stained for γ-tubulin or DNA. **B.** Pole to pole distance quantified following γ-tubulin staining in scramble (n=11) and UNC-45A (n=12) shRNAs transduced HeLa cells. **C.** Metaphase plate width quantified following DNA staining in scramble (n=11) and UNC-45A (n=12) shRNA transduced HeLa cells. **D.** Representative images of misaligned (arrow) chromosomes in HeLa cells transduced with either scramble or UNC-45A shRNAs and stained for DNA. **E.** Quantification of misaligned chromosomes per each condition (scramble n=77, UNC-45A knockdown n=80). **F.** Representative images of lagging (arrow) chromosomes in HeLa cells transduced with either scramble or UNC-45A shRNA and stained for DNA. **G**. Quantification of lagging chromosomes per each condition (scramble n=100, UNC-45A knockdown n=83). **H.** Representative images of multipolar spindles in HeLa cells transduced with either scramble or UNC-45A shRNA and stained for γ-tubulin or DNA. **I.** Quantification of percentage of cells with multipolar spindles per each condition. **J.** Representative images of normal (*left*) versus abnormal (*right*) mitotic figures in clinical specimens stained by immunohistochemistry for UNC-45A. **K.** Quantification of UNC-45A staining intensity correlated to the absence (no, n=35) or the presence (yes, n=13) of mitotic abnormalities.

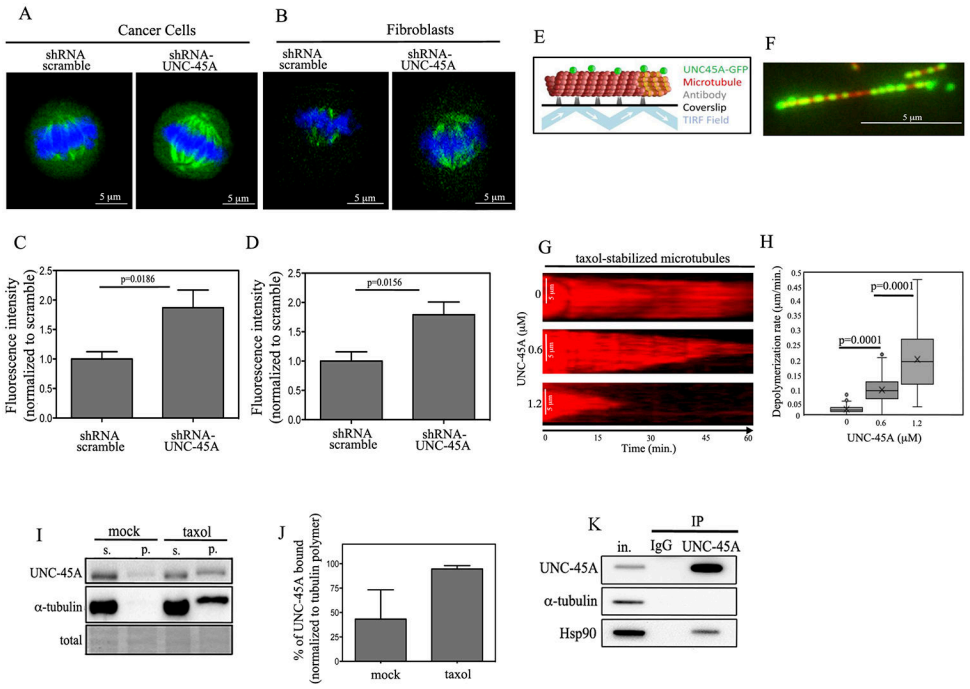


**Figure 5. UNC-45A is a microtubule destabilizing protein in cells and *in vitro*.**

(**A** and **B**). Representative images of HeLa (**A**) and NIH3T3 (**B**) cells either scramble or UNC-45A shRNA transduced and stained for acetylated α-tubulin (green) and DAPI (blue). **C.** Quantification of fluorescence intensity per each condition in HeLa cells (scramble n=8, UNC-45A knockdown n=8). **D.** Quantification of fluorescence intensity per each condition in NIH3T3 cells (scramble n=7, UNC-45A knockdown n=10). **E**. Experimental setup for TIRF microscopy examination of *in vitro* binding and depolymerization behavior of UNC-45A-GFP. Paclitaxel-stabilized (red) MTs are adhered to a coverslip with anti-rhodamine antibody, and then binding of (green) UNC-45A-GFP is visualized using TIRF microscopy. **F**. Example image of paclitaxel-stabilized MT (red) and UNC-45A-GFP (green). **G.** Kymograph representing time-lapse movie of paclitaxel-stabilized MT in the control experiment without UNC-45A. *Middle and bottom*, examples kymographs demonstrating depolymerization of taxol-stabilized MTs in presence of increasing concentrations of UNC-45A-GFP. **H.** Paclitaxel-stabilized MT depolymerization rates with increasing concentrations of UNC-45A-GFP (controls n=115; 0.6 μM n=138; 1.2 μM n=134; $p<0.0001$, controls vs 0.6 μM and 1.2 μM). **I.** MTs from COV362 cells stabilized in presence or in absence (mock) of 1μM taxol for 1 hour prior being subjected to ultracentrifugation. The resulting supernatant and pellet fractions were separated, fractionated by SDS-PAGE and subjected to Western blot analysis using anti UNC-45A and anti-α-tubulin antibodies. **J.** Quantification of % of UNC-45A bound normalized to tubulin polymer. **K**. UNC-45A immunoprecipitated from COV362 cell lysates with an anti-UNC-45A monoclonal antibody. Co-immunoprecipitated Hsp90 was detected by Western blot and used as positive control. Immunoprecipitation with mouse IgG was performed as a negative control.

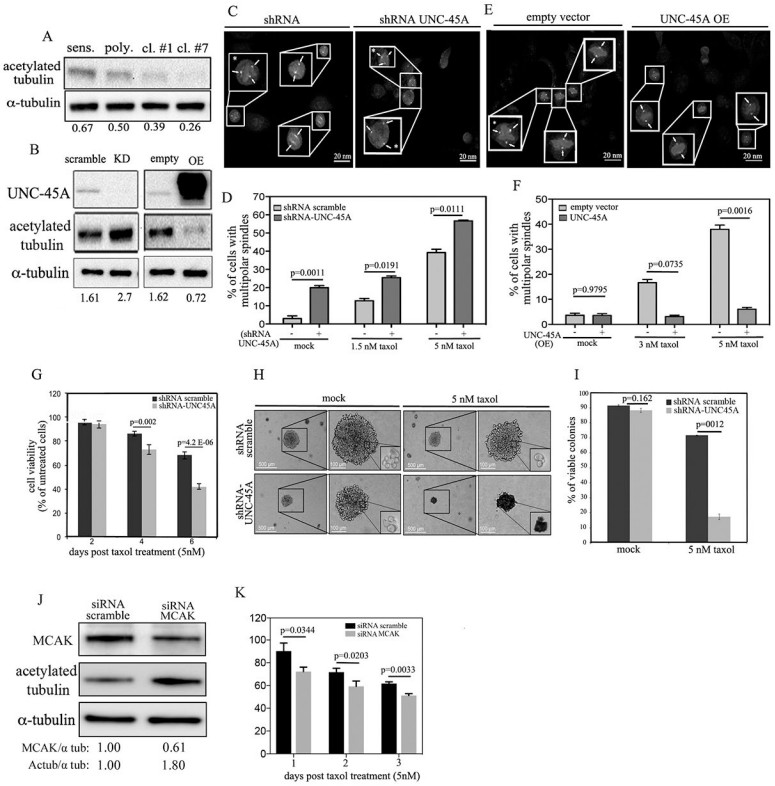


**Figure 6. UNC-45A depletion exacerbates paclitaxel-mediated stabilizing effects on mitotic spindles and restores sensitivity to paclitaxel.**

**A.** Western blot analysis for levels of UNC-45A acetylated α-tubulin in paclitaxel-sensitive and paclitaxel-resistant (polyclonal, clone #1, and clone #7) COV362 ovarian cancer cells. Numbers indicate the ratio between UNC-45A and α-tubulin. **B.** *Left,* Western blot analysis for levels of UNC-45A acetylated α-tubulin in COV362 ovarian cancer cells transduced with either shRNA scramble or shRNA-UNC-45A. Numbers indicate the ratio between acetylated α-tubulin and α-tubulin. *Right,* Western blot analysis for levels of UNC-45A in COV362 ovarian cancer cells infected with either empty vector (empty) or UNC-45A (overexpressing, OE). Numbers indicate the ratio between acetylated α-tubulin and α-tubulin. **C.** Mitotic figures containing multipolar spindles in either shRNA scramble or shRNA UNC-45A knockdown COV362 ovarian cancer cells in presence of 5 nM of paclitaxel as evaluated by γ-tubulin and DAPI staining. Arrows indicate spindle poles. Asterisks indicate cells with multipolar spindles. **D.** Quantification of cells containing multipolar spindles per each condition (mock: (−) n=20, (+) n=34; 1.5 nM paclitaxel: (−) n=23, (+) n=26; 5 nM paclitaxel: (−) n=29, (+) n=26). **E.** Mitotic figures containing multipolar spindles in either empty vector or UNC-45A overexpressing (OE) COV362 ovarian cancer cells in presence of 5 nM of paclitaxel as evaluated by α-tubulin and DAPI staining. Arrows indicate spindle pole. Asterisks indicate cells with multipolar spindles. **F.** Quantification of cells containing multipolar spindles per each condition (mock: (−) n=26, (+) n=37; 3 nM paclitaxel: (−) n=29, (+) n=31; 5 nM paclitaxel: (−) n=28, (+) n=32). **G.** Residual cell viability of shRNA scramble and shRNA-UNC45A knockdown COV362 cells exposed to 5nM paclitaxel over a period of 6 days. **H.** Equal numbers of shRNA scramble and shRNA-UNC- 45A SKOV-3

cells were seeded in soft agar for a period of 10 days prior paclitaxel treatment (5nM) over a period of three weeks. Per each condition, colonies were visualized using an inverted scope. Residual cell viability per each condition was evaluated in colonies' biopsies via trypan-blue exclusion assay. All experiments were conducted in triplicates. **I.** Quantification of residual cell viability per each condition (mock: shRNA scramble n=83, shRNA UNC-45A n=75; 5 nM paclitaxel: shRNA scramble n=60, shRNA UNC-45A n=52). **L.** Western blot analysis for levels of MCAK and acetylated α-tubulin in siRNA scramble versus siRNA MCAK treated COV362 cells. Numbers indicate the ratio between MCAK and alpha-tubulin or acetylated alpha-tubulin and alpha-tubulin. **M.** Residual cell viability of siRNA scramble and siRNA-MCAK COV362 cells exposed to 5nM paclitaxel over a period of three days.

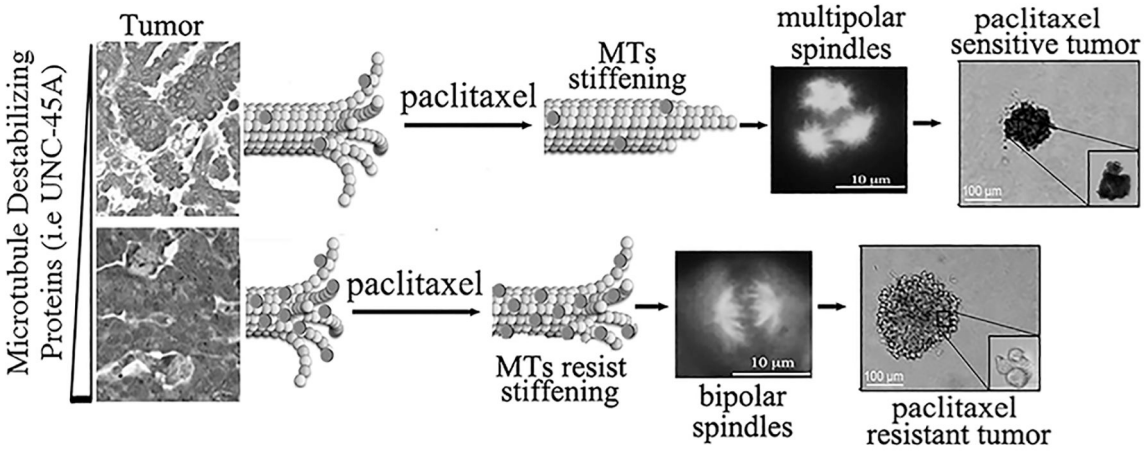


**Figure 7. Our findings identify UNC-45A as a master regulator of MT stability and paclitaxel-chemoresistance.**

*In situ*, overexpression of microtubule destabilizing proteins like UNC-45A (round dots) protects cancer cells from the stabilizing effects caused by paclitaxel. Cancer cells overexpressing UNC-45A escape paclitaxel-induced chromosomal missegregation on multipolar spindles and cell death.